
Generation of Parametric Image of Regional Myocardial Blood Flow Using H₂¹⁵O Dynamic PET and a Linear Least-Squares Method

Jae Sung Lee, PhD^{1,2}; Dong Soo Lee, MD, PhD¹; Ji Young Ahn, PhD¹; Jeong Seok Yeo, MD¹; Gi Jeong Cheon, MD¹; Seok-Ki Kim, MD¹; Kwang Suk Park, PhD^{1,2}; June-Key Chung, MD¹; and Myung Chul Lee, MD¹

¹Department of Nuclear Medicine, Seoul National University College of Medicine, Seoul, Korea; and ²Department of Biomedical Engineering, Seoul National University College of Medicine, Seoul, Korea

Although a parametric image of myocardial blood flow (MBF) can be obtained from H₂¹⁵O PET using factor and cluster analysis, this approach is limited when factor analysis fails to extract each cardiac component. In this study, a linear least-squares (LLS) method for estimating MBF and generating a MBF parametric image was developed to overcome this limitation. The computer simulation was performed to investigate the statistical properties of the LLS method, and MBF values obtained from the MBF parametric images in dogs were compared with those obtained using the conventional region of interest (ROI) and invasive microsphere methods. **Methods:** A differential model equation for H₂¹⁵O in the myocardium was modified to incorporate the partial-volume and spillover effect. The equation was integrated from time 0 to each PET sampling point to obtain a linearized H₂¹⁵O model equation. The LLS solution of this equation was estimated and used to calculate the MBF, the perfusable tissue fraction (PTF), and the arterial blood volume fraction (V_a). A computer simulation was performed using the input function obtained from canine experiments and the tissue time-activity curves contaminated by various levels of Poisson noise. The parametric image of the MBF, PTF, and V_a was constructed using the PET data from dogs ($n = 7$) at rest and after pharmacologic stress. The regional MBF from the parametric image was compared with those produced by the ROI method using a nonlinear least-squares (NLS) estimation and an invasive radio-labeled microsphere technique. **Results:** The simulation study showed that the LLS method was better than the NLS method in terms of statistical reliability, and the parametric images of the MBF, PTF, and V_a using the LLS method had good image quality and contrast. The regional MBF values using the parametric image showed a good correlation with those using the ROI method ($y = 0.84x + 0.40$; $r = 0.99$) and the microsphere technique ($y = 0.95x + 0.29$; $r = 0.96$). The computation time was approximately 10 s for the $32 \times 32 \times 6 \times 18$ (pixel \times pixel \times plane \times frame) matrix. **Conclusion:** A noninvasive, very fast, and accurate method for estimating the MBF and generating a MBF parametric image was developed using the LLS estimation technique and H₂¹⁵O dynamic myocardial PET.

Key Words: PET; H₂¹⁵O; myocardial blood flow; parametric image; linear least squares

J Nucl Med 2005; 46:1687–1695

Although qualitative perfusion SPECT provides valuable information on the diagnosis and management of coronary artery disease patients, quantitative perfusion imaging with PET plays an important role in examining diffuse myocardial diseases, such as microvessel disease, triple-vessel disease, or cardiomyopathy (1). Among the PET tracers for myocardial perfusion imaging, H₂¹⁵O is attractive because it is almost entirely extracted from the blood during its first pass across the myocardium and is not metabolized. Furthermore, the short half-life of ¹⁵O facilitates repeated or combined measurements with other tracers, which make this tracer more suitable for perfusion reserve measurements (2–5).

Despite the advantageous features of H₂¹⁵O for noninvasive and quantitative measurements of regional myocardial blood flow (rMBF), the generation of a pixel-wise parametric image of MBF using H₂¹⁵O PET is difficult to accomplish because of the low signal-to-noise ratio (SNR) of the time-activity curves of the individual pixels and the complicated kinetic modeling equation for the tissue time-activity curves (6,7). To overcome these problems in producing the MBF parametric images, a 2-step approach—in which factor analysis and cluster analysis were applied sequentially to dynamic H₂¹⁵O PET data—was previously suggested (8). First, using factor analysis, spillover contamination on the tissue time-activity curves from the ventricular blood-pool activity was eliminated. Second, cluster analysis was applied to the spillover-free tissue time-activity curves for the fast generation of a MBF parametric image. Although the feasibility of this method was validated in animal studies with a bolus injection of H₂¹⁵O, the use of this method is limited when factor analysis fails to separate the cardiac components. For example, when H₂¹⁵O is slowly infused and the MBF is increased by either exercise or

Received Feb. 1, 2005; revision accepted Jul. 11, 2005.
For correspondence contact: Dong Soo Lee, MD, PhD, Department of Nuclear Medicine, Seoul National University College of Medicine, 28 Yungun-Dong, Chongno-Ku, Seoul 110-744, Korea.
E-mail: dsl@plaza.snu.ac.kr

pharmacologic intervention, factor analysis sometimes cannot separate the ventricular blood-pool activities from the tissue time-activity curves because they have similar curves.

To overcome this limitation, this study adopted a linear least-squares (LLS) method for estimating MBF and generating a MBF parametric image. The LLS method and its generalized formula (generalized LLS: GLLS) for the dynamic PET data were originally established as fast algorithms for determining the cerebral blood flow and the cerebral glucose metabolism (9,10). Chen et al. modified these algorithms to incorporate correction factors for the bidirectional spillover effects in myocardial PET studies and applied this method to $^{13}\text{NH}_3$ PET data (11). The aim of this study was to (a) derive LLS equations to describe the kinetic model of H_2^{15}O PET, (b) evaluate the statistical properties of the LLS method to estimate MBF using computer simulation, (c) generate parametric images of MBF and its related parameters using this method, and (d) validate the parametric imaging method by comparing the rMBF values obtained using the parametric image with those using the conventional region of interest (ROI) method and the invasive microsphere method.

MATERIALS AND METHODS

Theory

The ideal kinetic model for H_2^{15}O in the tissue without partial-volume and spillover effects is given by the following equation:

$$\frac{dC_T}{dt} = f \cdot C_a(t) - fp \cdot C_T(t) = f \cdot C_a(t) - k_2 \cdot C_T(t), \quad \text{Eq. 1}$$

where $C_a(t)$ and $C_T(t)$ are the ideal input functions of time t ($\mu\text{Ci/mL}$) and the tissue time-activity curve ($\mu\text{Ci/g}$), respectively. f is the myocardial blood flow that is free of a partial-volume effect (MBF_p , mL/min/g); p is the tissue-blood partition coefficient, which was fixed as 0.91 mL/g ; and k_2 ($\equiv fp$) is the quotient of the MBF_p and partition coefficient (6,7,12).

The measured input function and tissue time-activity curves by PET can be related to the ideal ones by these 2 equations by incorporating the partial-volume and spillover effects:

$$\tilde{C}_a(t) = C_a(t). \quad \text{Eq. 2}$$

$$\tilde{C}_T(t) = \alpha \cdot C_T(t) + V_a \cdot C_a(t). \quad \text{Eq. 3}$$

α is the perfusable tissue fraction (PTF, g/mL) or recovery coefficient for the partial-volume correction of the tissue time-activity curve, and V_a is the arterial blood volume fraction (mL/mL) of the ROI (6,7,12). It was assumed that the left ventricular (LV) input function is free of partial-volume and spillover effects because such a LV input function could be obtained either by averaging the time-activity curves from the ROIs, which were drawn on the center of the LV cavity across several midventricular slices and small enough to avoid spillover contamination from the myocardial activity, or by applying factor analysis or other similar methods (13-15).

Therefore, the ideal time-activity curves can be expressed with the measured time-activity curves according to the following equations:

$$C_a(t) = \tilde{C}_a(t). \quad \text{Eq. 4}$$

$$C_T(t) = \frac{\tilde{C}_T(t) - V_a \cdot \tilde{C}_a(t)}{\alpha}. \quad \text{Eq. 5}$$

Substituting the Equations 4 and 5 into Equation 1, and multiplying both sides by α :

$$\frac{d}{dt} \{ \tilde{C}_T(t) - V_a \cdot \tilde{C}_a(t) \} = K_1 \cdot \tilde{C}_a(t) - k_2 \{ \tilde{C}_T(t) - V_a \cdot \tilde{C}_a(t) \}, \quad \text{Eq. 6}$$

where K_1 ($\equiv \alpha f$) is the product of MBF_p and PTF, and is called MBF_t (mL/min/mL). A kinetic modeling equation for H_2^{15}O in the tissue can be derived by rearranging this equation with the measured time-activity curves as follows:

$$\frac{d\tilde{C}_T(t)}{dt} = P_1 \cdot \frac{d\tilde{C}_a(t)}{dt} + P_2 \cdot \tilde{C}_a(t) + P_3 \cdot \tilde{C}_T(t). \quad \text{Eq. 7}$$

$$\begin{aligned} P_1 &\equiv V_a, \\ P_2 &\equiv K_1 + k_2 \cdot V_a, \\ P_3 &\equiv -k_2. \end{aligned} \quad \text{Eq. 8}$$

The macroparameters, P_1 , P_2 , and P_3 , can be obtained using the LLS method (Appendix), and each microparameter required is given by the following equations:

$$\begin{aligned} V_a &= P_1, \\ k_2 &= fp = -P_3, \quad f = -P_3 \cdot p, \\ K_1 &= \alpha \cdot f = P_2 + P_1 \cdot P_3, \quad \alpha = (P_2 + P_1 \cdot P_3)/f. \end{aligned} \quad \text{Eq. 9}$$

Simulation Study

A computer simulation was performed to investigate the statistical properties of the LLS method using the simulated input function and tissue time-activity curves contaminated by various levels of Poisson noise. Noiseless tissue time-activity curves were generated using the single-compartment model by applying the average LV input function obtained from canine experiments. The subsequent sections explain the methods used to perform the canine experiments and obtain the individual input function. In brief, the individual LV input function was obtained by drawing small circular ROI on the central region of the LV cavity in the myocardium factor image obtained in previous canine studies using factor analysis (8). To generate the average LV input function, each LV input function was normalized to the peak activity, interpolated at every 0.1 s, shifted in the time domain so that the times to reach the peak were the same in all cases, and resampled using the same sampling time as the original LV input function ($5 \text{ s} \times 12$, $10 \text{ s} \times 6$). The PTF, p , and V_a values were fixed at 0.55 g/mL , 0.91 mL/g , and 0.2 mL/mL , respectively. The MBF_p value was varied between 1.0 and $\sim 4.0 \text{ mL/min/g}$. Pseudorandom noise was added to each frame of the tissue time-activity curve to simulate noisy measurements. The Poisson noise was simulated by assuming that the measurement error variance is proportional to the radioactivity and inversely proportional to the scan length: The variance in counts of the i th frame was described as follows:

$$\sigma^2(t_i) = Sc \cdot \tilde{C}_T(t_i) / \delta t_i, \quad \text{Eq. 10}$$

where Sc is the scaling factor and δt_i is the scan length of the i th frame. The scaling factor that determines the level of noise was varied from 0 to 2.0. Ten thousand datasets (noisy tissue time-

activity curves) were generated for all simulations at each noise level. The MBF_p values were estimated using the nonlinear least squares (NLS) and LLS methods, and the coefficient of the variation (CV), error, and bias in the estimation of MBF_p were calculated as follows:

$$CV = \frac{\sigma(f_{est})}{\bar{f}_{est}} \times 100 (\%), \quad \text{Eq. 11}$$

$$Error = \left[\sum_{i=1}^N \frac{|f_{est,i} - f_{true}|}{f_{true}} \times 100 (\%) \right] / N, \quad \text{Eq. 12}$$

$$Bias = \left[\sum_{i=1}^N \frac{f_{est,i} - f_{true}}{f_{true}} \times 100 (\%) \right] / N, \quad \text{Eq. 13}$$

where \bar{f}_{est} and $\sigma(f_{est})$ are the mean and SD of the estimated MBF_p , $f_{est,i}$ estimated MBF_p with the i th noisy dataset, and f_{true} true MBF_p .

Canine Experimental Data

To validate the MBF parametric image generated using the LLS method under the resting condition and during drug-induced hyperemia, this method was applied retrospectively to canine experimental data acquired in previous studies (8,13–15). The $H_2^{15}O$ PET scans were obtained on 7 adult normal mongrel dogs weighing, on average, 22.5 kg at rest ($n = 7$) and after pharmacologic stress using either adenosine or dipyridamole ($n = 5$). All scans were acquired using an ECAT EXACT 47 scanner (Siemens-CTI), featuring 47 simultaneous contiguous planar images with a 3.4-mm thickness for a longitudinal field of view of 16.2 cm. Before administering the $H_2^{15}O$, transmission scanning was performed using three ^{68}Ge rod sources to correct the photon attenuation. Dynamic emission scans (5 s \times 12, 10 s \times 9, 30 s \times 3) were initiated simultaneously with the injection of 555–740 MBq $H_2^{15}O$ and continued for 4 min, and initial 2-min data were used for the MBF estimation. Transaxial images were reconstructed using a filtered backprojection algorithm using a Shepp–Logan filter with a cutoff frequency of 0.3 cycle/pixel, as 128 \times 128 \times 47 matrices with a size of 2.57 \times 2.57 \times 3.38 mm.

To compare the rMBF obtained using $H_2^{15}O$ PET, MBF was measured using 15.5- μ m-diameter radiolabeled microspheres (NEN Life Science Products, Inc.) in 6 of the 7 dogs scanned at rest and 4 of the 5 dogs scanned after stress. Simultaneously with the injection of water through a forelimb vein, the microspheres labeled with either ^{46}Sc , ^{85}St , or ^{113}Sn were administered into the LV through a catheter inserted into the LV cavity via the femoral artery over a 10- to ~15-s period. The arterial blood was sampled for 2 min and the microsphere activity count was taken using a well counter (Cobra II, Packard Instrument Co., Inc.).

After sacrificing the dogs, the hearts were removed and sliced into 1-cm-thick LV short-axis cross-sections. The lowest one was regarded as the apex and the LV myocardium in the remaining 4 or 5 cross-sections was further divided into 4 segments (total, 17 or 21 segments per study)—namely, the anterior, lateral, and inferior regions, and the septum. By considering the position of the myocardium in the parametric images, each segment was defined in the following way: First, the interventricular sulci between the LV and right ventricular (RV) myocardium (insertion sites of the RV myocardium into the LV myocardium) were identified as septum-defining landmarks; the myocardium between these 2

points was defined as the septum. Second, the area symmetric to this septum in the cross-section, with respect to the long axis of the LV cavity, was defined as the lateral region. Third, the areas between the septum and lateral region were defined as the anterior and inferior regions. The regional blood flow of each segment was calculated using a standard microsphere reference technique (16).

Parametric Image Generation

The dynamic PET images were also reoriented to the short axis and then resampled to produce a 1-cm thickness to increase the SNR and have the same thickness and position as the tissue slices. Each frame of the dynamic images was reoriented using the parameters for rotation and the translation determined by the static images obtained by summing dynamic frames. The cardiac regions were then masked to remove the extracardiac components and reduce the calculation time. The mask size was 32 \times 32 \times 6 (pixel \times pixel \times plane).

The LV input function was obtained by drawing circular ROIs (~100 mm²), which were small enough to avoid spillover contamination from the myocardial activity, on the central regions of the LV cavities in the myocardium factor images obtained in a previous study using factor analysis (8) and were copied onto the original dynamic images. The LV input functions from the 2 ROIs on neighboring midventricular slices were averaged to reduce the statistical fluctuation. Parametric images of MBF_t ($K_1 = \alpha f$), PTF (α), and the arterial blood volume fraction (V_a) were generated using the LLS method by using this input function and the time–activity curves of every pixel after in-plane smoothing of the PET data with an isotropic gaussian kernel with a 4.0-mm full width at half maximum (FWHM) to reduce the statistical fluctuation in the pixel counts. Considering the low resolution of the PET scanner for ^{15}O (~10-mm FWHM) as a result of the relatively long positron range, degradation of the spatial resolution caused by the smoothing with the 4.0-mm gaussian kernel could not be significant (expected resolution after smoothing (square root of 10² + 4²) = 10.77 mm).

Comparison with Conventional Methods

To compare the rMBF values obtained by LLS parametric images with those using the conventional ROI and microsphere methods, polygonal ROIs were drawn on the myocardium factor images. The ROIs were drawn on the identical regions defined in the microsphere studies (the areas between the interventricular sulci as septum, the area symmetric to the septum as the lateral region, and the myocardium between the septum and lateral region as the anterior and inferior regions, respectively). The number of ROIs generated from the myocardium factor images was same as the number of ROIs generated from the microsphere analysis. To estimate the rMBF from the LLS parametric images, the mean MBF_t and PTF values of each ROI were calculated and the MBF_p value was obtained by dividing the mean MBF_t by the mean PTF.

For the rMBF estimation using the ROI method, each ROI was copied onto the original dynamic images to obtain the mean tissue time–activity curve within the ROI. The MBF_p values were estimated using a conventional NLS method with these time–activity curves and the same LV input functions that were used for generating the parametric image.

Five MBF values per study (anterior, lateral, inferior, septum, and apex) were obtained by averaging the MBF values from the same anatomic regions for all methods and compared with each other.

Statistical Analysis

The correlation coefficients of the MBF_p values obtained from the parametric images and those using the ROI method were calculated. Correlation analysis was also performed between MBF_p values from the parametric image and the MBF obtained using the microsphere technique. The mean and SD of the differences between paired measurements (PET methods minus microsphere) were calculated to evaluate the systematic error and random variability in the MBF estimation. To assess the significance of the systemic errors between the measurements, paired t tests between the MBF values were performed. Relative dispersion of $rMBF$ values (CV of the MBF for 5 anatomic regions) was estimated to assess the stability of each method and compared by ANOVA with the F test. Bonferroni correction was applied for the multiple-comparison correction, and results were considered significant at $P < 0.05$.

Preliminary Application to Human Data

To show the feasibility of the proposed method, the LLS parametric images of the MBF and related parameters were generated from the $H_2^{15}O$ PET data acquired from a male volunteer.

RESULTS

Simulation Study

The CV, bias, and error (%) in the MBF_p estimation calculated by the computer simulation were plotted against the noise level (Fig. 1). The CV, bias, and error were increased as the true MBF decreased and the noise level increased. The LLS showed lower CV, error, and bias than the NLS in most conditions. The reduction in the CV and error by the LLS method was approximately 35% and 25%, but the bias reduction was dependent on the true MBF level. The simulated data with $Sc = 0.5$ or $Sc = 1.0$ were correlated with the noise levels shown in each pixel of the

canine dynamic PET data (pixel size = $2.57 \times 2.57 \times 10.3$ mm³).

Parametric Images

Figures 2 and 3 show the parametric images of MBF_t , PTF, and the arterial blood volume fraction generated using the LLS method from the dynamic $H_2^{15}O$ PET studies on a dog at rest and after dipyridamole stress, respectively. The uniform distribution of blood flow on myocardium and the high contrast between myocardium and background structures could be identified from the parametric images of MBF_t . The increased MBF could be represented in the parametric image of the MBF_t after dipyridamole stress.

The computation time for generating the parametric images using the LLS method was approximately 10 s for the masked cardiac region ($32 \times 32 \times 6 \times 18$ pixel \times pixel \times plane \times frame) when the IDL (Interactive Data Language) language and Pentium 3 processor was used.

Comparison with Conventional Methods

The regional MBF (f , MBF_p) obtained by the ROI on the parametric images showed a strong correlation with that estimated using the mean tissue time-activity curve of the ROI and the NLS estimation (Fig. 4A) ($r = 0.99$; $y = 0.84x + 0.40$, $n = 60$). It also showed a good correlation with the gold standard values of the blood flow obtained using the radiolabeled microspheres (Fig. 4B) ($r = 0.96$; $y = 0.95x + 0.29$, $n = 50$). In particular, the y -intercepts in these correlation analyses were significantly lower than those obtained using the previous method with factor analysis, in which the same data as described in the current study were used (8) (0.82 with ROI method and 0.85 with microsphere method, which were almost the same as the

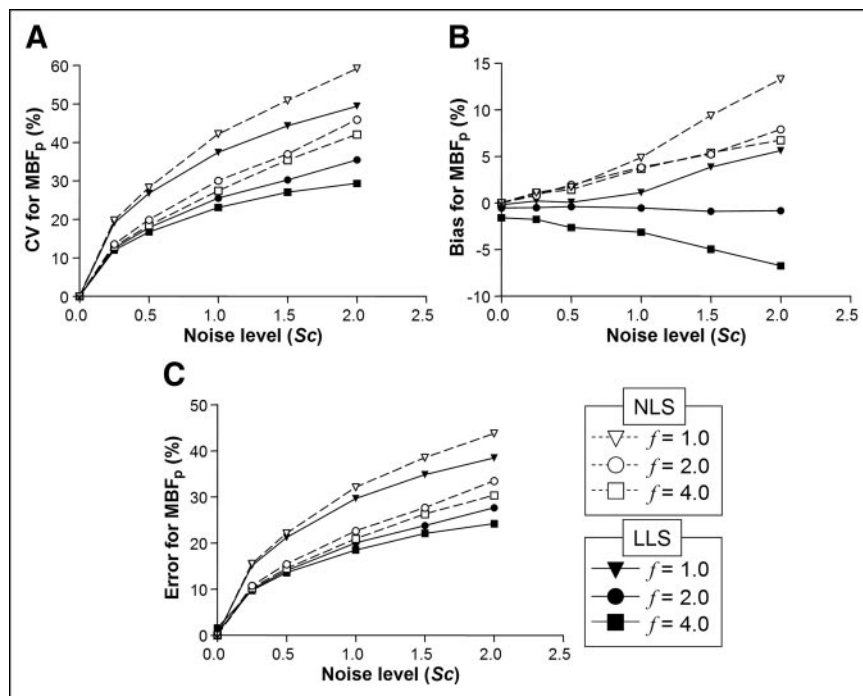


FIGURE 1. (A) CV, (B) bias, and (C) error in estimation of MBF_p (f) calculated by computer simulation.

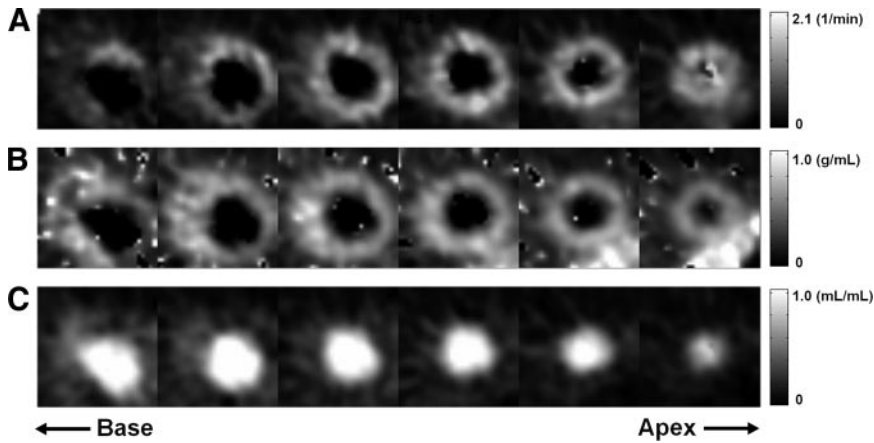


FIGURE 2. Parametric images generated using LLS method from dynamic $H_2^{15}O$ canine PET study at rest. (A) MBF_t ($\alpha \cdot f$). (B) PTF (α). (C) Arterial blood volume fraction (V_a).

normal resting flow and regarded as the major limitation of the previous method), and the correlation coefficients were higher (0.94 with ROI method and 0.90 with microsphere method in the previous study). The quality of the parametric images was also improved if they were compared with those shown by Lee et al. (8).

For comparison, the correlation between the rMBF values obtained using microspheres and the ROI method is shown in Figure 4C ($r = 0.96$; $y = 1.12x - 0.13$, $n = 50$). PTF values obtained from the LLS parametric images also showed a good correlation with that obtained using the conventional ROI method ($r = 0.94$; $y = 0.88x + 0.09$, $n = 60$).

The mean and SD of the differences between MBF values determined by the microspheres and the parametric image or ROI method are shown in the Table 1. The mean differences (systemic error) were not significant and the systemic errors of the parametric image and the ROI method also were not significantly different from each other (0.16 ± 0.53 vs. 0.18 ± 0.64 mL/min/g). Table 2 summarizes the relative dispersion of rMBF values within the whole myocardium for each method. Although the mean relative dispersion was smallest in the MBF values determined by the LLS parametric images, they were not significantly different.

Human Study: Preliminary Result

Figure 5 shows the parametric image of MBF_t generated from the rest $H_2^{15}O$ PET data of a healthy volunteer (body weight, 60 kg) after administration of 1,480 MBq of $H_2^{15}O$. The parametric image was superimposed on the static image that was obtained by summing dynamic frames from scan start to 4 min after the administration of $H_2^{15}O$.

DISCUSSION

This study developed a noninvasive, fast, and accurate method for estimating MBF and generating a MBF parametric image using the LLS estimation technique and $H_2^{15}O$ PET. A computer simulation study was performed to show the improvement in the statistical reliability of this method, and the MBF values obtained from the MBF parametric image were compared with those obtained using the conventional ROI and invasive microsphere methods.

The parametric images generated using the pixel-by-pixel calculation of the kinetic parameters are preferred because they are not constrained by the bias in the selection of a ROI. Moreover, they can facilitate a numeric evaluation and clinical interpretation of the MBF distribution (8,11,17,18). To generate a parametric image of the MBF from $H_2^{15}O$ PET, techniques using $C^{15}O$ blood-pool scan data and an

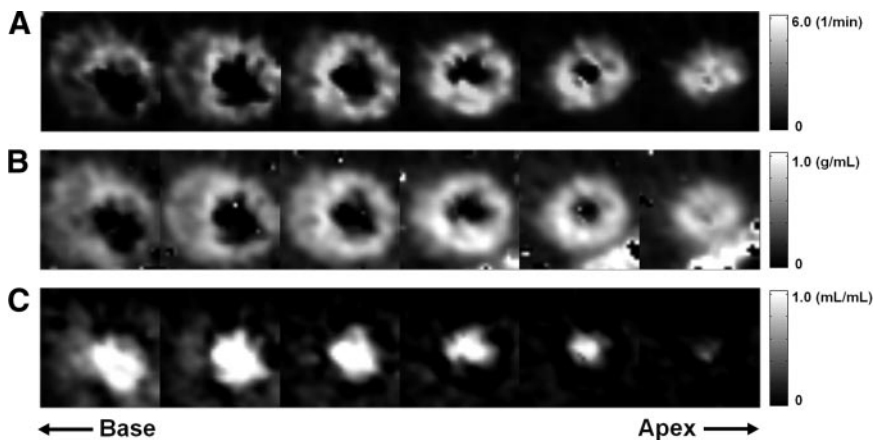


FIGURE 3. Parametric images generated by LLS method from dynamic $H_2^{15}O$ canine PET study after dipyridamole stress. (A) MBF_t ($\alpha \cdot f$). (B) PTF (α). (C) Arterial blood volume fraction (V_a).

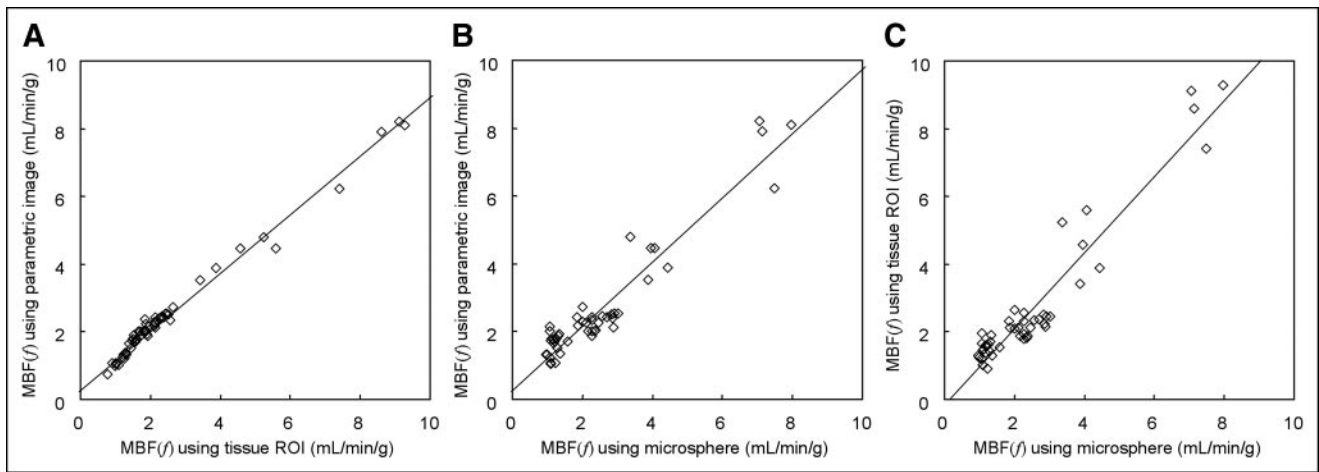


FIGURE 4. Correlation between MBF (f) values. (A) Parametric image vs. ROI method ($y = 0.84x + 0.40$; $r = 0.99$). (B) Parametric image vs. microsphere technique ($y = 0.95x + 0.29$; $r = 0.96$). (C) ROI method vs. microsphere technique ($y = 1.12x - 0.13$; $r = 0.96$).

autoradiographic method (19) or a weighted integration method (12) were suggested. However, to determine the MBF using the autoradiographic method, the value of the PTF needs to be fixed, commonly to 1 g/mL. Fixation of the PTF in this way produced a systemic underestimation of the MBF, and the calculated MBF became dependent on the accumulation time (19). In a later work by the same group (12), a weighted integration method (20,21) was applied after subtracting the arterial blood volume fraction estimated using the $C^{15}O$ and the transmission images from the dynamic frames with an assumed venous fraction in the myocardium (0.1 mL/g). However, variations in the venous fraction shown in their work were too high to be ignored (0.12 ± 0.08 and 0.08 ± 0.11 mL/g in lateral and anterior regions, respectively) (7). Moreover, the assumption of a fixed venous fraction was unjustified in some physiologic conditions. For example, under the hypertensive conditions induced by pharmacologic stress, the venous fraction increased approximately 3-fold. Another problem of these previous approaches relates to the erroneous MBF estimation, attributed to a misalignment between the $C^{15}O$ image and the other images, which limits the use of the $C^{15}O$ data for estimating the MBF and arterial blood volume fraction.

Improvements in image-processing techniques that are based on various multivariate data analyses (8,13–15,22–25) have led to the possible elimination of the additional $C^{15}O$ scan and the accompanying errors associated with the

use of $C^{15}O$ data in the $H_2^{15}O$ PET studies. In a previous study on generating a MBF parametric image (8), the LV input function was derived directly from the $H_2^{15}O$ dynamic PET using factor analysis without either $C^{15}O$ data or arterial blood sampling. The important advantage of factor analysis in the aspect of the parametric imaging was that the blood-pool activity obtained by factor analysis contained only the arterial blood volume fraction. Therefore, no assumption about the venous fraction was required. This was because the temporal variations in the venous activity were equal to those of the tissue activity because water behaved as a freely diffusible tracer. Accordingly, the blood-pool activities due to only the arterial blood volume fraction could be removed in each voxel, and a pixel-by-pixel MBF parametric image could be generated using the single-compartment model with only 2 parameters, in which the MBF estimation was facilitated by the cluster analysis (8). However, the use of this 2-step approach was limited by the unsuccessful separation of the blood-pool activity in some cases previously introduced along with the bias in the MBF estimation, which was found by a comparison with the MBF values obtained using the ROI-based approach and the microsphere method.

In this study, the application of a 1-step generation of the parametric image using the modified LLS method significantly reduced such bias in the MBF estimation. Moreover, the computer simulation study demonstrated that the statis-

TABLE 1
Differences Between MBF Determined by PET and Microspheres (mL/min/g)

Method	n	Mean difference (systemic error)	SD (random variability)	t test
Parametric (LLS), microsphere	50	0.16	0.53	NS
ROI (NLS), microsphere	50	0.18	0.64	NS

NS = not significant.

TABLE 2
Relative Dispersion (CV of MBF Values for 5 Anatomic Regions) of Different Methods

Parameter	Method			
	Microsphere	Parametric (LLS)	ROI (NLS)	ANOVA
Mean \pm SD	0.20 \pm 0.10	0.19 \pm 0.05	0.22 \pm 0.08	NS

NS = not significant.

tical reliability in the MBF estimation by the LLS method was also improved in comparison with the conventional NLS method. It has been shown many times that error and CV in MBF estimation increase with increasing MBF as the difference between the arterial input function and tissue time-activity curve becomes smaller. Our simulation results would be different from the previous reports primarily because a different definition of the noise level was used. In the previous studies, the percentage of the SD of the gaussian-shaped noise at the maximum of the noise-free time-activity curve (the % noise level) was used to describe the level of the noise. If the time-activity curves have the same percentage noise level regardless of the MBF, the CV will increase with increasing MBF. However, this assumption would not be appropriate because the percentage noise level increases with lower MBF. The amplitude and SNR of the tissue time-activity curves with lower MBF decrease because of the Poisson characteristics of the noise. Therefore, we generated more realistic pseudorandom Poisson noise, in which the measurement error variance was proportional to the radioactivity and inversely proportional to the scan length. The decrease of the SNR with lower MBF would be dominant over the influence of the similarity of time-activity curves.

Although the LLS method showed lower CV, error, and bias than the NLS method in most conditions, the reduction of bias was dependent on the true MBF level and the bias with the LLS method was worse than the NLS method for hyperemic flow. The magnitude of the negative bias obtained for MBF of 4 mL/min/g with LLS (Fig. 1B, ■) was slightly greater than the magnitude of the positive bias obtained for MBF of 4 mL/min/g using NLS (Fig. 1B, □). In addition, the relationship between the magnitude of bias and MBF level was not linear: There was very little bias with LLS for MBF of 2 mL/min/g, with bias becoming

negative as MBF increases and positive as MBF decreases. The complex nature of the bias in the MBF estimated by the LLS method can be partially explained by the dependency of the error terms in integrated equations. The LLS solution shown in Equation 7A was obtained with the assumption that the error terms in Equation 6A were mutually independent. However, the assumption would not be true because the integration periods overlap so that the later error terms contain the previous errors (9,10). This dependency between error terms leads to bias in the estimated parameters when the LLS method is used. The GLLS method was suggested to overcome this problem of bias (9). However, according to our experience, the GLLS method was not efficient enough to reduce the bias, although the computation time increased approximately 3-fold (26).

The validation of this method was limited to MBF measurements under the resting condition and during drug-induced hyperemia. Therefore, further validation of this method for MBF measured under ischemic and infarction conditions along with an investigation of the utility in assessing clinical data will be necessary. In addition, systematic investigations should be performed to show the feasibility of the proposed method in generation of the MBF parametric image from the human H₂¹⁵O PET data because generation of the MBF image is more difficult for human data than canine data because of the larger magnitude of attenuation and scatter and higher noise level in human data. The noise level in human dynamic PET data was approximately correlated with the simulated data with $S_c = 1.5$ or 2.0, although the canine data were correlated with $S_c = 0.5$ or 1.0.

The current method only takes into account the spillover from the LV (Eq. 3), although the time-activity curve of the RV has a different shape (27,28). Therefore, the spillover effects in the septum would not be corrected sufficiently.

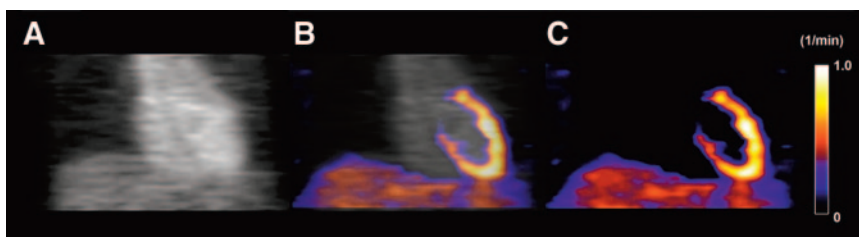


FIGURE 5. Parametric image of MBF_t generated from rest H₂¹⁵O PET data of healthy volunteer. (A) Static image. (B) MBF_t($\alpha \cdot f$) parametric image superimposed on static image. (C) MBF_t parametric image.

Extension of the current method to include the RV spillover correction in the myocardial septum is a mathematically simple task: 2 more terms will be added in the right side of the Equation 1A. Further investigations to evaluate the effects of such incorporation of the RV spillover term in the LLS method on the MBF and PTF estimation in the septum would be required.

CONCLUSION

A noninvasive, very fast, and accurate method for estimating the MBF and generating a MBF parametric image was developed using the LLS estimation technique and $H_2^{15}O$ dynamic myocardial PET.

APPENDIX

LLS Method

The following n equations were obtained by integrating Equation 7 from time 0 to each PET sampling point t_i ($i = 1, \dots, n$):

$$\begin{aligned}\tilde{C}_T(t_1) &= P_1 \cdot \tilde{C}_a(t_1) + P_2 \int_0^{t_1} \tilde{C}_a(\tau) d\tau + P_3 \int_0^{t_1} \tilde{C}_T(\tau) d\tau. \\ \tilde{C}_T(t_2) &= P_1 \cdot \tilde{C}_a(t_2) + P_2 \int_0^{t_2} \tilde{C}_a(\tau) d\tau + P_3 \int_0^{t_2} \tilde{C}_T(\tau) d\tau. \\ &\vdots \\ \tilde{C}_T(t_n) &= P_1 \cdot \tilde{C}_a(t_n) + P_2 \int_0^{t_n} \tilde{C}_a(\tau) d\tau + P_3 \int_0^{t_n} \tilde{C}_T(\tau) d\tau.\end{aligned}$$

Eq. 1A

These equations can be considered to be a set of linear equations in which the arterial input function, the time integrations of the input function, and the tissue time-activity curves are independent variables, and the tissue time-activity curve is a dependent variable. P_1 , P_2 , and P_3 are coefficients. Rearranging these equations into a matrix gives the following equation:

$$\mathbf{y} = \mathbf{X}\boldsymbol{\theta} + \boldsymbol{\epsilon}, \quad \text{Eq. 2A}$$

where \mathbf{y} is a vector for the dependent variable, \mathbf{X} is the matrix for the independent variables, $\boldsymbol{\theta}$ is a vector for the parameters to be estimated, and $\boldsymbol{\epsilon}$ is the equation error term:

$$\mathbf{y} \equiv [\tilde{C}_T(t_1) \quad \tilde{C}_T(t_2) \quad \dots \quad \tilde{C}_T(t_n)]^T. \quad \text{Eq. 3A}$$

$$\mathbf{X} \equiv \begin{bmatrix} \tilde{C}_a(t_1) & \int_0^{t_1} \tilde{C}_a(\tau) d\tau & \int_0^{t_1} \tilde{C}_T(\tau) d\tau \\ \tilde{C}_a(t_2) & \int_0^{t_2} \tilde{C}_a(\tau) d\tau & \int_0^{t_2} \tilde{C}_T(\tau) d\tau \\ \vdots & \vdots & \vdots \\ \tilde{C}_a(t_n) & \int_0^{t_n} \tilde{C}_a(\tau) d\tau & \int_0^{t_n} \tilde{C}_T(\tau) d\tau \end{bmatrix}. \quad \text{Eq. 4A}$$

$$\boldsymbol{\theta} \equiv [P_1 \quad P_2 \quad P_3]^T. \quad \text{Eq. 5A}$$

$$\boldsymbol{\epsilon} \equiv [\epsilon_1 \quad \epsilon_2 \quad \dots \quad \epsilon_n]^T. \quad \text{Eq. 6A}$$

An estimate of $\boldsymbol{\theta}$ based on the LLS criterion is given by the following equation:

$$\hat{\boldsymbol{\theta}}_{LLS} = (\mathbf{X}^T \mathbf{X})^{-1} \mathbf{X}^T \mathbf{y}. \quad \text{Eq. 7A}$$

ACKNOWLEDGMENTS

This work was supported by the Basic Atomic Energy Research Institute program and by the Brain Korea 21 program for Human Life Sciences. The authors thank Dr. Hideiro Iida at the National Cardiovascular Center Research Institute, Osaka, for his valuable comments and helpful discussions on the various topics, including the change of venous fraction under the hypertensive conditions.

REFERENCES

- Tamaki N, Kuge Y, Tsukamoto E. The road to quantitation of regional myocardial uptake of tracer. *J Nucl Med.* 2001;42:780–781.
- Bergmann SR, Fox KAA, Rand AL, et al. Quantification of regional myocardial blood flow in vivo with $H_2^{15}O$. *Circulation.* 1984;70:724–733.
- Araujo LI, Lammertsma AA, Rhodes CG, et al. Noninvasive quantification of regional myocardial blood flow in coronary artery disease with oxygen-15-labeled carbon dioxide inhalation and positron emission tomography. *Circulation.* 1991;83:875–885.
- Lammertsma AA, De Silva R, Araujo LI, Jones T. Measurement of regional myocardial blood flow using $C^{15}O_2$ and positron emission tomography: comparison of tracer models. *Clin Phys Physiol Meas.* 1992;13:1–20.
- Bol A, Melin JA, Vanoverschelde J-L, et al. Direct comparison of $[^{13}N]$ ammonia and $[^{15}O]$ water estimates of perfusion with quantification of regional myocardial blood flow by microspheres. *Circulation.* 1993;87:512–525.
- Herrero P, Markham J, Myears DW, Weiheimer CJ, Bergmann SR. Measurement of myocardial blood flow with positron emission tomography: correction for count spillover and partial volume effects. *Math Comput Model.* 1988;11:807–812.
- Iida H, Christopher GR, Ranil S, et al. Myocardial tissue fraction-correction for partial volume effects and measure of tissue viability. *J Nucl Med.* 1991;32:2169–2175.
- Lee JS, Lee DS, Ahn JY, et al. Parametric image of myocardial blood flow generated from dynamic $H_2^{15}O$ PET using factor analysis and cluster analysis. *Med Biol Eng Comput.* In press.
- Feng D, Wang Z, Huang S-C. A study on statistically reliable and computationally efficient algorithms for generating local cerebral blood flow parametric images with positron emission tomography. *IEEE Trans Med Imaging.* 1993;12:182–188.
- Feng D, Huang S-C, Wang Z, Ho D. An unbiased parametric imaging algorithm for nonuniformly sampled biomedical system parameter estimation. *IEEE Trans Med Imaging.* 1996;15:512–518.
- Chen K, Lawson M, Reiman E, et al. Generalized linear least squares method for fast generation of myocardial blood flow parametric images with N-13 ammonia PET. *IEEE Trans Med Imaging.* 1998;17:236–243.
- Iida H, Tamura Y, Kitamura K, et al. Histochemical correlates of ^{15}O -water-perfusible tissue fraction in experimental canine studies with old myocardial infarction. *J Nucl Med.* 2000;41:1737–1745.
- Ahn JY, Lee DS, Lee JS, et al. Quantification of regional myocardial blood flow using dynamic $H_2^{15}O$ PET and factor analysis. *J Nucl Med.* 2001;42:782–787.
- Lee JS, Lee DS, Ahn JY, et al. Blind separation of cardiac components and extraction of input function from $H_2^{15}O$ dynamic myocardial PET using independent component analysis. *J Nucl Med.* 2001;42:938–943.
- Lee JS, Lee DD, Choi S, Park KS, Lee DS. Non-negative matrix factorization of dynamic images in nuclear medicine. *Proc IEEE Nucl Sci Symp Med Imaging Conf.* 2001;4:2027–2030.
- Heymann MA, Payne BD, Hoffman JI, Rudolph AM. Blood flow measurements with radionuclide-labeled particles. *Prog Cardiovasc Dis.* 1977;20:55–79.
- Choi Y, Huang S-C, Hawkins RA, et al. A simplified method for quantification of myocardial blood flow using nitrogen-13-ammonia and dynamic PET. *J Nucl Med.* 1993;34:488–497.

18. Gewirtz H. Parametric images for quantitative measurements of regional myocardial blood flow in humans: a step in the right direction. *J Nucl Med.* 1993;34:862–864.
19. Iida H, Kanno I, Takahashi A, et al. Measurement of absolute myocardial blood flow with $H_2^{15}O$ and dynamic positron-emission tomography: strategy for quantification in relation to the partial-volume effect. *Circulation.* 1988;78:104–115.
20. Alpert NM, Eriksson L, Chang JY, et al. Strategy for the measurement of regional cerebral blood flow using short-lived tracers and emission tomography. *J Cereb Blood Flow Metab.* 1984;4:28–34.
21. Koeppe RA, Holden JE, Ip WR. Performance comparison of parameter estimation techniques for the quantitation of local cerebral blood flow by dynamic positron computed tomography. *J Cereb Blood Flow Metab.* 1985;5:224–234.
22. Wu HM, Hoh CK, Buxton DB, et al. Quantification of myocardial blood flow using dynamic nitrogen-13-ammonia PET studies and factor analysis of dynamic structures. *J Nucl Med.* 1995;36:2087–2093.
23. Hermansen F, Ashburner J, Spinks TJ, et al. Generation of myocardial factor images directly from the dynamic oxygen-15-water scan without use of an oxygen-15-carbon monoxide blood-pool scan. *J Nucl Med.* 1998;39:1696–1702.
24. Frouin F, Merlet P, Bouchareb Y, et al. Validation of myocardial perfusion reserve measurements using regularized factor images of $H_2^{15}O$ dynamic PET scans. *J Nucl Med.* 2001;42:1737–1746.
25. Sitek A, Gullberg GT, Huesman RH. Correction for ambiguous solutions in factor analysis using a penalized least squares objective. *IEEE Trans Med Imaging.* 2002;21:216–225.
26. Lee JS, Lee DS, Park KS, Chung JK, Lee MC. Comparison of algorithms for generating parametric image of cerebral blood flow using $H_2^{15}O$ positron emission tomography. *Korean J Nucl Med.* 2003;37:288–300.
27. Hermansen F, Rosen SD, Fath-Ordoubadi F, et al. Measurement of myocardial blood flow with oxygen-15 labelled water: comparison of different administration protocols. *Eur J Nucl Med.* 1998;25:751–759.
28. Hove JD, Gambhir SS, Kofoed KF, Kelbaek H, Schelbert HR, Phelps ME. Dual spillover problem in the myocardial septum with nitrogen-13-ammonia flow quantitation. *J Nucl Med.* 1998;39:591–598.

